https://doi.org/10.20965/ijat.2021.p0215

Paper:

Forward Kinematics Model for Evaluation of Machining Performance of Robot Type Machine Tool

Akio Hayashi*,†, Hiroto Tanaka*, Masato Ueki, Hidetaka Yamaoka*, Nobuaki Fujiki*, and Yoshitaka Morimoto***

*Kanazawa Institute of Technology
7-1 Ohgigaoka, Nonoichi, Ishikawa 924-8501, Japan
†Corresponding author, E-mail: a-hayashi@neptune.kanazawa-it.ac.jp
**Sumitomo Wiring Systems, Ltd., Yokkaichi, Japan

[Received August 31, 2020; accepted December 1, 2020]

Robot-type machine tools are characterized by the ability to change the tool posture and machine itself with a wider motion range than conventional machine tools. The motion of the robot machine tool is realized by simultaneous multi-axis control of link mechanisms. However, when the robot machine tool performs a general milling process, some problems that affect the machining accuracy occur. Moreover, it is difficult to identify the motion errors of each axis, which influence machining accuracy. Thus, it is difficult to adjust the servo gain and alignment error. In addition, the machining performance is unidentified because of the rigidity differences when the posture changes. In this study, the focus was on robot-type machine tools consisting of a serial and a parallel link mechanism. A geometric model is described, and the forward kinematics model is derived based on the geometric model. Machining tests were then carried out to evaluate the machining accuracy by measuring the machined surfaces and the simulated motion of the tool posture based on the proposed forward kinematics model to identify the mechanism that affects the machined surface roughness and surface waviness. As a result, it was shown that the proposed model can separate and reproduce the behavior of each axis of the machine. Finally, it was clarified that the behavior of the second axis has a great influence on the tool posture and machined surface.

Keywords: robot-type machine tools, parallel link mechanism, forward kinematics model, positioning accuracy, machining performance

1. Introduction

With the advocacy of "Industry 4.0" and recent changes and trends in production equipment, robots are expected to be used widely not only for conventional transportation but also for processing because of the diversification of processing machines. Considering the control and high precision of these robots as well as the connection between physical space and cyber space, modeling of machine tools has become an extremely important issue [1, 2].

Robot-type machine tools are expected to be used not only for machining and grinding, but also for welding. Robot-type machine tools have the feature that the tool tip posture can be directed in any direction by a parallel mechanism. Furthermore, various processes are made possible by attaching a spindle, a spot welding device, a grinding wheel, etc. to the end effector. By using this feature, it is possible to machine a large product, such as the wings of an aircraft, by positioning the robot-type machine tool on a large guide-way because some robot-type machine tools are lighter than conventional machine tools, and it is easy to change their position [3–6]. Robot-type machine tools have two main types of mechanism. The first is a serial link mechanism. In this mechanism, the tool posture and position are determined by the links and joints of the robots connected in series. The other is a parallel link mechanism, which often determines the position of the link plate by driving multiple links in parallel. As a result, the tool tip can be positioned in various directions. Thus, a parallel mechanism is used in various machines for robots and manipulators, not only machine tools [7–12].

However, the positioning accuracy may be reduced owing to the complexity of the machine structure and errors in the assembly and motion of each part. Therefore, many researchers have studied their application and use. Because motion accuracy directly affects machining accuracy in machine tools, many precision measurement techniques for machine tools with multiple axes, such as five-axis machine tools, are currently being studied [13–18]. Because the parallel mechanism is a more complicated axis mechanism, it is possible for not only the motion accuracy but also the rigidity to change depending on the mechanism and posture of the machine.

Several studies have been conducted on parameter correction to improve the accuracy of parallel mechanism machine tools [19–24]. In the present study, a kinematic model and a method of calibrating mechanical parame-

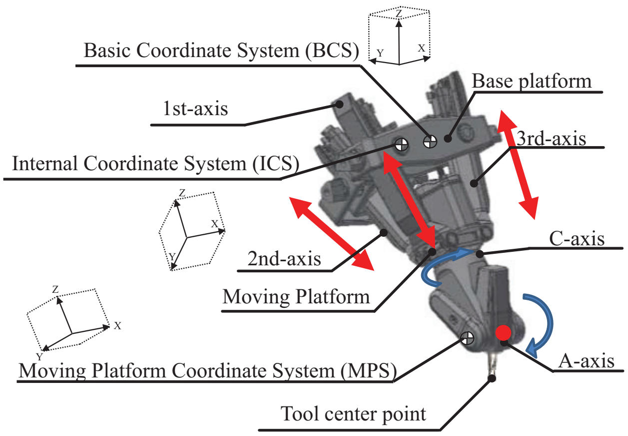

Fig. 1. Schematic diagram of robot type machine tool.

ters using an arm coordinate measuring machine are proposed [25]. The effect of calibration was evaluated by simulation and by machining and motion tests. In this method, the motion accuracy is improved by calculating the correction value repeatedly. However, in this method, because the correction values for all the mechanisms are calculated and converged at the same time, it is unknown which parameter has a large influence to machine errors. This method is expected to be useful to determine the machining performance of the machine and its characteristics separately and to improve it.

Thus, in this study, a three-dimensional (3D) geometric model was derived for a robot-type machine tool having a structure combining the serial and parallel link mechanisms described above, and the mechanism of the machine tool was modeled. Based on the model, a forward kinematics model to calculate the tool chip position was derived. Then, to evaluate the machining performance of the machine tool, machining tests were performed. From the machining results and the motion of each axis of the machine tool, the factor that influences the machined surface characteristics was revealed.

2. Forward Kinematics Model of Robot-Type Machine Tool with Parallel and Serial Link Mechanisms

2.1. Geometric Model and Origins of Robot-Type Machine Tool

Figure 1 shows a schematic diagram of the robot-type machine tool (XMini, Exechon Enterprises, LLC). The machine tool was controlled by SINUMERIK 840D (Simens AG). The machine tool consists of a parallel link mechanism (1st-axis, 2nd-axis, and 3rd-axis), which moves with linear motion and is set to the base platform. The serial link mechanism of the rotational *C*- and *A*-axes is set on the moving platform.

There are three coordinate systems to represent this machine tool with a forward kinematics model. The first one is the basic coordinate system (BCS) on the base platform. The second is the internal coordinate system (ICS) that takes into account the tilt of the entire machine. This coordinate system has been rotationally transformed by *A*-axis rotation, which is the rotation around the *X*-axis of the BCS, and the origin O_{ICS} exists at the intersection of the base platform and the first axis. The third is the moving platform coordinate system (MPS), which takes into account the tilt of the moving platform as shown in **Fig. 1**. The inclination of this coordinate system changes in various directions depending on the lengths of the first, second, and third axes, which are the linear motion axes. This change in the slope of the coordinate system has a significant effect on deriving the *C*- and *A*-axis angles. The origin O_{MPS} of this coordinate system is on the *C*-axis, and the line connecting the origin and the *A*-axis is perpendicular to the *C*-axis.

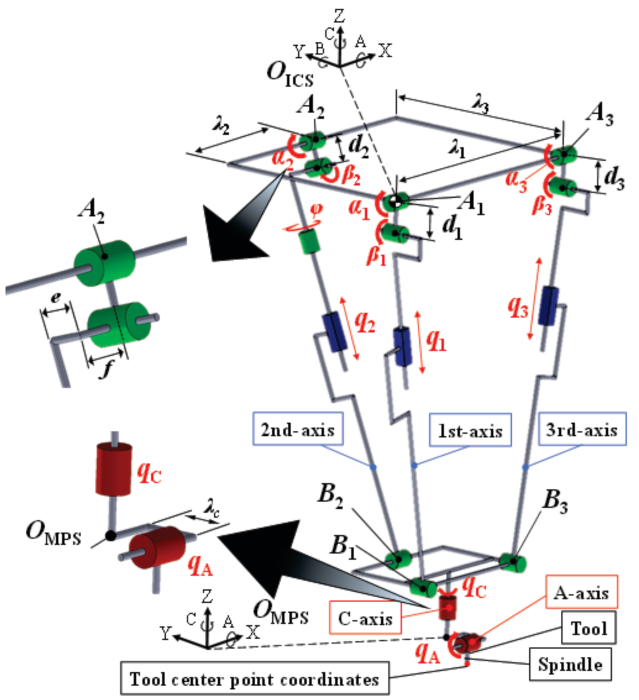

Fig. 2. Geometric model of machine tool.

2.2. Forward Kinematics Model

The 3D geometric model of the machine tool is shown in **Fig. 2** to visualize the parameters with the direction and offset value considered in the motion controller program. Here, q_1, q_2, q_3, q_c, and q_a are parameters that can be specified numerically on the controller, and the other rotational axes are free. They vary depending on the posture. Parameters q_i, d_1, d_2, d_3, e, f, λ_1, λ_2, and λ_3 indicate the offsets between the axes. The FARO Gage, which is a 3D measurement device for the offsets and coordinate acquisition, was used based on xCAL software provided by Exechon Enterprises, LLC. Previous research has shown a calculation method to simply this offset value calculation and improve accuracy [25].

The forward kinematics model is derived based on the shape generation theory using a homogeneous coordinate transformation matrix $\boldsymbol{A}_n$ [26].

First, a forward kinematics model for the first axis and the $\boldsymbol{B}_1$ coordinates are derived. The first axis is expressed by Eq. (1) because the origin of the ICS coordinate system is on $\boldsymbol{A}_1$ and there is no offset on the base platform. Here, $\boldsymbol{R}(\alpha_1)$ indicates the rotational coordinate of the first axis around the X-axis, $\boldsymbol{D}_1$ is the offset from the outer joint to the inner joint, and $\boldsymbol{R}(\beta_1)$ is the rotational coordinate of the first axis around the Y-axis. In addition, $\boldsymbol{Q}_1$ indicates the stroke of the first axis.

$$\begin{aligned}\boldsymbol{B}_1 &= \boldsymbol{R}(\alpha_1)\boldsymbol{D}_1\boldsymbol{R}(\beta_1)\boldsymbol{Q}_1\\ &= \begin{bmatrix}1&0&0&0\\0&\cos(\alpha_1)&-\sin(\alpha_1)&0\\0&\sin(\alpha_1)&\cos(\alpha_1)&0\\0&0&0&1\end{bmatrix}\begin{bmatrix}1&0&0&0\\0&1&0&0\\0&0&1&-d_1\\0&0&0&1\end{bmatrix}\\ &\quad\begin{bmatrix}\cos(\beta_1)&0&\sin(\beta_1)&0\\0&1&0&0\\-\sin(\beta_1)&0&\cos(\beta_1)&0\\0&0&0&1\end{bmatrix}\begin{bmatrix}0\\0\\-q_1\\1\end{bmatrix} \quad . \ . \quad (1)\end{aligned}$$

Similarly, the $\boldsymbol{B}_2$ and $\boldsymbol{B}_3$ coordinates of the second axis and the third axis are expressed in Eqs. (2) and (3).

$$\begin{aligned}\boldsymbol{B}_2 &= \boldsymbol{A}_2\boldsymbol{R}(\alpha_2)\boldsymbol{D}_2\boldsymbol{R}(\beta_2)EFR(\phi)\boldsymbol{Q}_2\\ &= \begin{bmatrix}1&0&0&\lambda_2\\0&1&0&\lambda_3\\0&0&1&0\\0&0&0&1\end{bmatrix}\begin{bmatrix}1&0&0&0\\0&\cos(\alpha_2)&-\sin(\alpha_2)&0\\0&\sin(\alpha_2)&\cos(\alpha_2)&0\\0&0&0&1\end{bmatrix}\\ &\quad\begin{bmatrix}1&0&0&0\\0&1&0&0\\0&0&1&-d_2\\0&0&0&1\end{bmatrix}\begin{bmatrix}\cos(\beta_2)&0&\sin(\beta_2)&0\\0&1&0&0\\-\sin(\beta_2)&0&\cos(\beta_2)&0\\0&0&0&1\end{bmatrix}\\ &\begin{bmatrix}1&0&0&-f\\0&1&0&e\\0&0&1&0\\0&0&0&1\end{bmatrix}\begin{bmatrix}\cos(\phi)&-\sin(\phi)&0&0\\\sin(\phi)&\cos(\phi)&0&0\\0&0&1&0\\0&0&0&1\end{bmatrix}\begin{bmatrix}0\\0\\-q_2\\1\end{bmatrix}\\ &\quad . \quad (2)\end{aligned}$$

$$\begin{aligned}\boldsymbol{B}_3 &= \boldsymbol{A}_3\boldsymbol{R}(\alpha_3)\boldsymbol{D}_3\boldsymbol{R}(\beta_3)\boldsymbol{Q}_3\\ &= \begin{bmatrix}1&0&0&0\\0&1&0&0\\0&0&1&\lambda_1\\0&0&0&1\end{bmatrix}\begin{bmatrix}1&0&0&0\\0&\cos(\alpha_3)&-\sin(\alpha_3)&0\\0&\sin(\alpha_3)&\cos(\alpha_3)&0\\0&0&0&1\end{bmatrix}\\ &\begin{bmatrix}1&0&0&0\\0&1&0&0\\0&0&1&-d_3\\0&0&0&1\end{bmatrix}\begin{bmatrix}\cos(\beta_3)&0&\sin(\beta_3)&0\\0&1&0&0\\-\sin(\beta_3)&0&\cos(\beta_3)&0\\0&0&0&1\end{bmatrix}\begin{bmatrix}0\\0\\-q_3\\1\end{bmatrix}\\ &\quad . \quad (3)\end{aligned}$$

First, the $\boldsymbol{O}_M$ coordinates are derived using the $\boldsymbol{B}_1$ coordinates shown in Eq. (4). This is done using the defined tilt of the moving platform and the distance from $\boldsymbol{O}_M$ to $\boldsymbol{B}_1$ in MPS. In addition, the $\boldsymbol{O}_M$ coordinates are derived in the same calculation process in the $\boldsymbol{B}_2$ and $\boldsymbol{B}_3$ coordinates. Because the external rotation angle α and the internal rotation angle β are required, they must be derived. Because the same coordinates are obtained regardless of the axis, the $\boldsymbol{O}_M$ coordinates are obtained, and simultaneous equations are derived.

In addition, the tilt on the base platform is not considered in the above equations. Therefore, the fact that the $\boldsymbol{O}_M$ coordinates can be obtained from the $\boldsymbol{B}_1$, $\boldsymbol{B}_2$, and $\boldsymbol{B}_3$ coordinates is used to derive the tilt using the following simultaneous equations, where $\boldsymbol{O}_{MB1}$ is the $\boldsymbol{O}_M$ coordinate obtained from the first axis, $\boldsymbol{O}_{MB2}$ is the $\boldsymbol{O}_M$ coordinate obtained from the second axis, and $\boldsymbol{O}_{MB3}$ is the $\boldsymbol{O}_M$ coordinate obtained from the third axis.

$$\begin{aligned}\boldsymbol{O}_M &= \boldsymbol{B}_i\boldsymbol{R}(\theta_{MPYZ})\boldsymbol{R}(\theta_{MPXZ})\boldsymbol{O}_M\boldsymbol{B}_i\\ &= \begin{bmatrix}1&0&0&B_{iX}\\0&1&0&B_{iY}\\0&0&1&B_{iZ}\\0&0&0&1\end{bmatrix}\\ &\quad\begin{bmatrix}1&0&0&0\\0&\cos(\theta_{MPYZ})&-\sin(\theta_{MPYZ})&0\\0&\sin(\theta_{MPYZ})&\cos(\theta_{MPYZ})&0\\0&0&0&1\end{bmatrix}\\ &\quad\begin{bmatrix}\cos(\theta_{MPXZ})&0&\sin(\theta_{MPXZ})&0\\0&1&0&0\\-\sin(\theta_{MPXZ})&0&\cos(\theta_{MPXZ})&0\\0&0&0&1\end{bmatrix}\begin{bmatrix}O_MB_{iX}\\O_MB_{iY}\\O_MB_{iZ}\\1\end{bmatrix}\\ &\quad (i=1,2,3) \quad . \ . \ . \ . \ . \ . \ . \ . \ . \ . \ . \ . \ . \quad (4)\end{aligned}$$

$$\boldsymbol{O}_{MB1} = \boldsymbol{O}_{MB2} = \boldsymbol{O}_{MB3} \quad . \ . \ . \ . \ . \ . \ . \ . \ . \ . \ . \quad (5)$$

When the $\boldsymbol{B}_1$, $\boldsymbol{B}_2$, and $\boldsymbol{B}_3$ coordinates have been calculated, the inclination of the moving platform and the position of the origin on the moving platform can be derived. Based on these results, it is possible to derive the tool tip coordinates $\boldsymbol{S}$, as described in Eq. (6).

$$\begin{aligned}\boldsymbol{S} &= \boldsymbol{R}(\theta_0)\boldsymbol{O}_M\boldsymbol{R}(\theta_{CYZ})\boldsymbol{R}(\theta_{CXZ})\boldsymbol{R}(q_c)\boldsymbol{L}_c\boldsymbol{R}(q_A)\boldsymbol{T}\\ &= \begin{bmatrix}1&0&0&0\\0&\cos(\theta_0)&-\sin(\theta_0)&0\\0&\sin(\theta_0)&\cos(\theta_0)&0\\0&0&0&1\end{bmatrix}\begin{bmatrix}1&0&0&O_{MX}\\0&1&0&O_{MY}\\0&0&1&O_{MZ}\\0&0&0&1\end{bmatrix}\\ &\quad\begin{bmatrix}1&0&0&0\\0&\cos(\theta_{CYZ})&-\sin(\theta_{CYZ})&0\\0&\sin(\theta_{CYZ})&\cos(\theta_{CYZ})&0\\0&0&0&1\end{bmatrix}\\ &\quad\begin{bmatrix}\cos(\theta_{CXZ})&0&\sin(\theta_{CXZ})&0\\0&1&0&0\\-\sin(\theta_{CXZ})&0&\cos(\theta_{CXZ})&0\\0&0&0&1\end{bmatrix}\\ &\quad\begin{bmatrix}\cos(q_c)&-\sin(q_c)&0&0\\\sin(q_c)&\cos(q_c)&0&0\\0&0&1&0\\0&0&0&1\end{bmatrix}\begin{bmatrix}1&0&0&0\\0&1&0&\lambda_C\\0&0&1&0\\0&0&0&1\end{bmatrix}\\ &\quad\begin{bmatrix}1&0&0&0\\0&\cos(q_A)&-\sin(q_A)&0\\0&\sin(q_A)&\cos(q_A)&0\\0&0&0&1\end{bmatrix}\begin{bmatrix}-t_X\\-t_Y\\-t_Z\\1\end{bmatrix} \quad . \ . \ . \quad (6)\end{aligned}$$

The behavior of the tool tip can be confirmed by inputting encoder information during the actual operation of a specific axis in this model. Furthermore, the error in each direction is estimated by comparing it with the

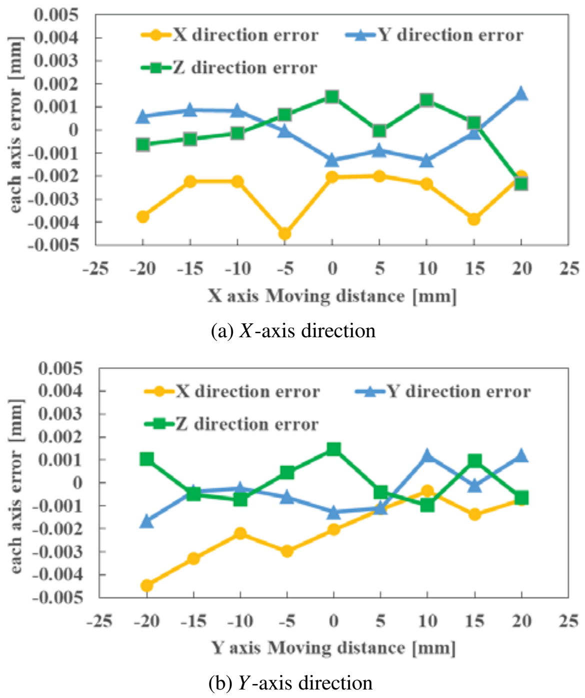

Fig. 3. Error of simulated results of machine motion.

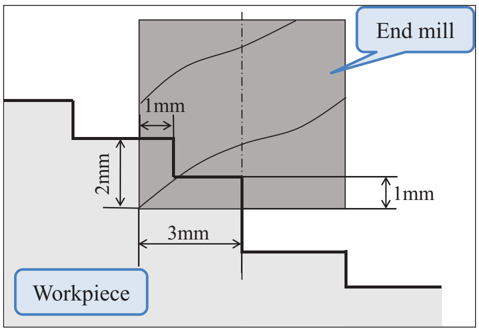

Fig. 4. Schematic diagram of cutting area.

commanded position of the tool tip. A linear motion of ± 20 mm was performed at 5 mm intervals in the X- and Y-axis directions. **Fig. 3** shows the error in the simulated results of the tool tip position for the linear motion in X- and Y-axis directions. These results show that the maximum error is less than 5 μm in the X-axis direction, which is a high simulation accuracy. These results demonstrate that the proposed model can simulate the tool tip position from the motion of each axis.

3. Machining Tests and Evaluation of Machining Accuracy

Machining tests were carried out with a square end mill in the X- and Y-axis directions on the BCS, and the surface properties were measured to evaluate the machining performance. **Fig. 4** shows the area processed by the square end mill. **Table 1** lists the machining conditions.

Table 1. Machining condition.

Conditions		Value	Unit
Spindle speed		5000	min^{-1}
Feed		150	mm/min
Cutting		92.4	m/min
Coolant		Dry cut	-
End mill diameter		6	mm
Depth of cut	Axial	1	mm
	Radial	1	mm
Milling direction		Down cut	-

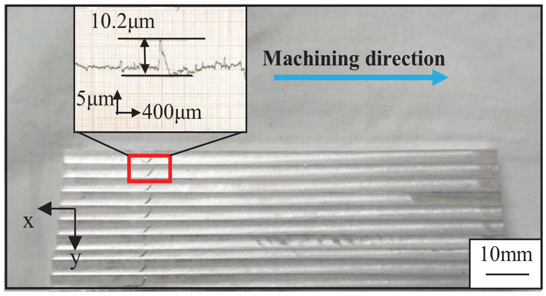

Fig. 5. Machined surface by end mill in X-direction.

3.1. Machining Result in X-Axis Direction

Figure 5 shows the machined surface and the maximum height roughness of down-cut machining in the X-axis direction on the BCS. From this result, the machine elements that affect the machining surface properties are specified by observing the behaviors of the machine tool and the tool tip point.

The part surrounded by the square in **Fig. 5** in the machined surface in the X-axis direction shows the cutter mark (between 10 and 11 s of machining). The mark is on the surface machined by the bottom blade of the end mill. This contact mark also appears on the surface machined by the side blade. The maximum height of this contact mark is 10.2 μm, which is not good for a machined surface.

To investigate the cause of cutter marks, the motion of each axis of the robot machine tool was measured using an external encoder and the internal function of the controller. **Fig. 6** shows the motion of each axis. As a result, the reversal motion of the servo motor was observed on the second axis and the A-axis around the representative cutter mark. **Figs. 7(a)** and **(b)** show the enlarged view of measured motions of the second and A-axis during reversal motion, respectively. The second axis moves approximately 10 μm.

Figures 8(a) and **(b)** show the calculated results of the tool tip position around the reversal motion based on the proposed forward kinematics model. It was calculated by inputting the measured motion of each axis (as shown in **Fig. 7**) into the equations. As a result, it was clarified that a displacement of approximately 30 μm occurs in the Y-axis direction, as shown in **Fig. 8(a)**. Furthermore,

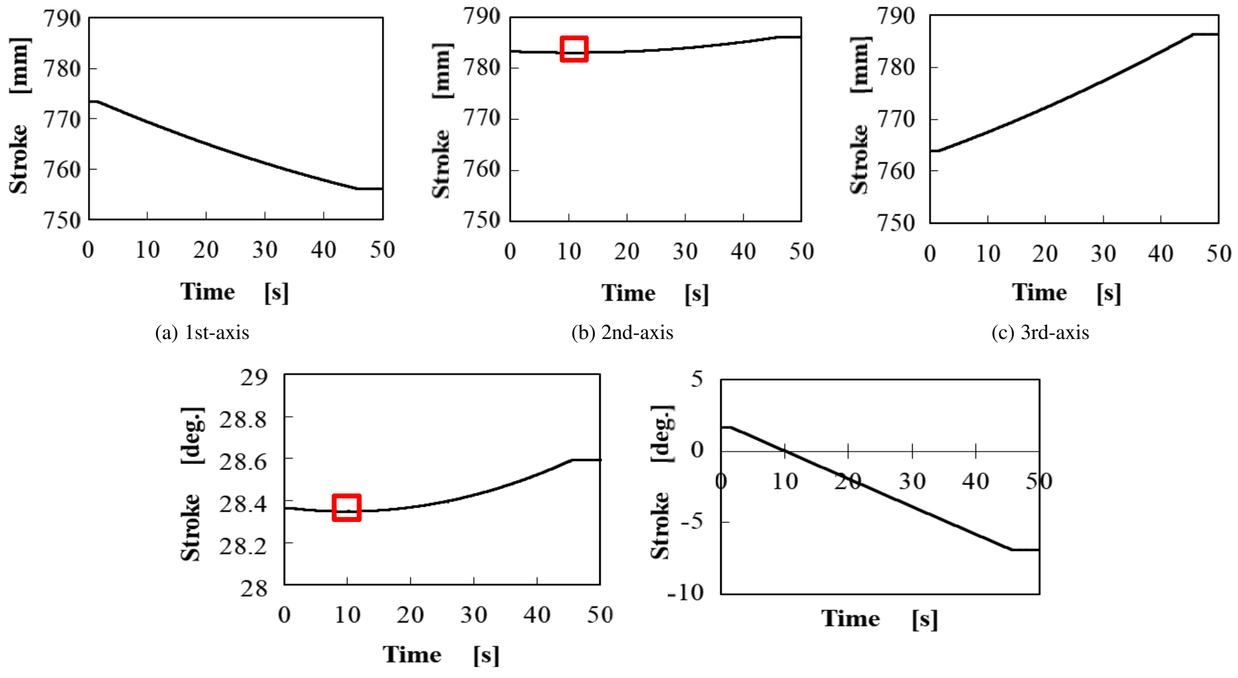

(a) 1st-axis (b) 2nd-axis (c) 3rd-axis

(d) *A*-axis (e) *C*-axis

Fig. 6. Each axis motion behavior in *X*-direction machining.

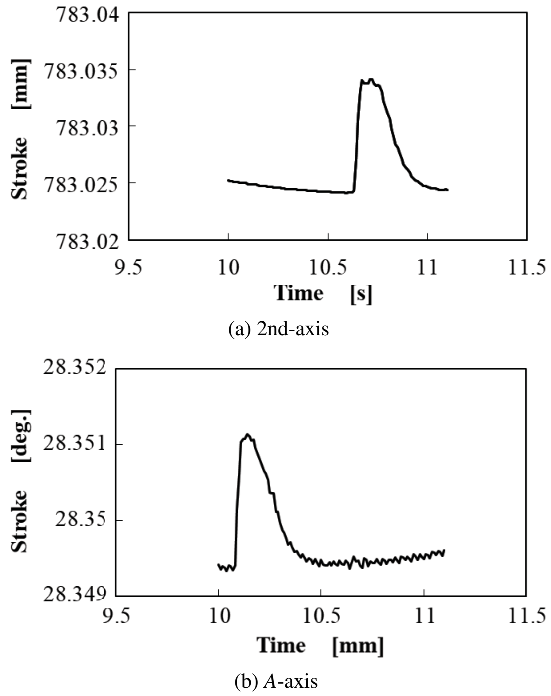

(a) 2nd-axis

(b) *A*-axis

Fig. 7. Measured motion of each axis around cutter marks.

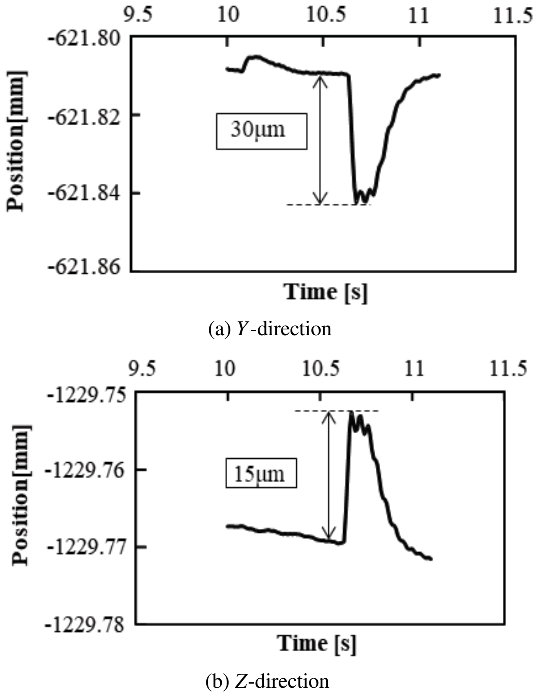

(a) *Y*-direction

(b) *Z*-direction

Fig. 8. Calculated results of tool chip position.

as shown in **Fig. 8(b)**, a displacement of approximately 15 μm occurs in the *Z*-axis direction.

Thus, to clarify which axis, the *A*-axis or the second axis, has a greater effect on this motion error, one axis substitutes the theoretical motion and the other axis substitutes the measured motion of each axis.

Here, theoretical motion means that it is assumed that the axis motion does not cause the protrusion phenomenon at the time of reversal motion as shown in **Fig. 7**, and it is processed by an approximated curve. **Figs. 9(a)** and **(b)** show the simulated results of the tool chip position obtained by the above method. **Fig. 9(a)** shows a case where only the motion of the second axis is predicted, and **Fig. 9(b)** shows a case where only the motion of the

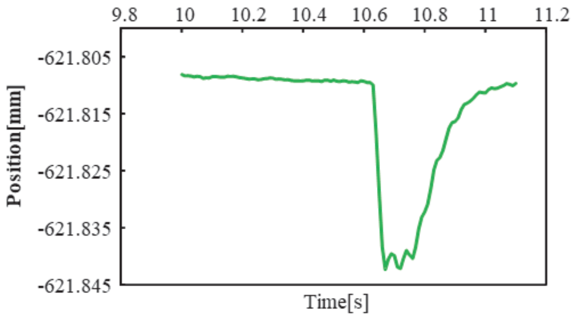

(a) 2nd-axis

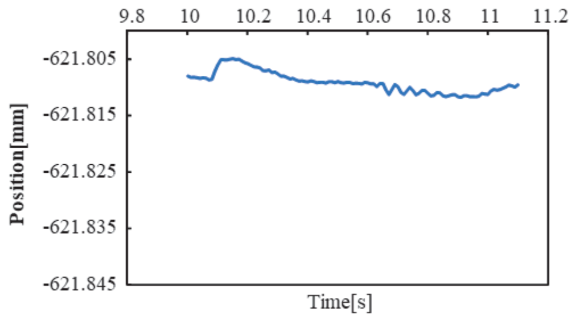

(b) *A*-axis

Fig. 9. Calculated results of tool chip position by separating influence of each axis motion (*Y*-direction machining process).

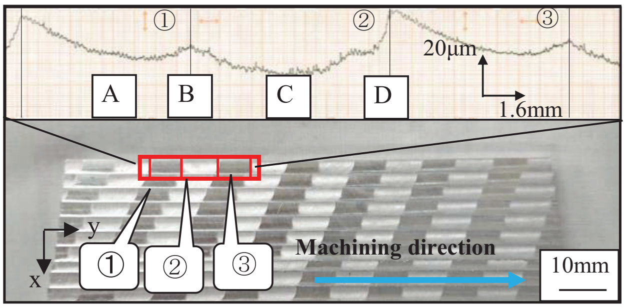

Fig. 10. Machined surface in *Y*-direction process.

(a) Surface A (b) Surface B (c) Surface C (d) Surface D

Fig. 11. Enlarged surface in *Y*-direction process.

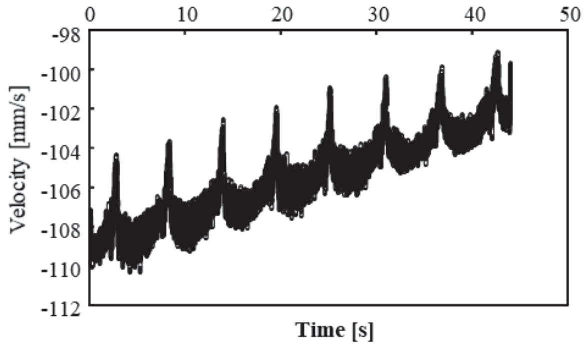

Fig. 12. Moving velocity of 2nd-axis.

A-axis is predicted.

These results demonstrated that a small movement error of approximately 3 μm in the vicinity of 10–10.2 s was the influence of the *A*-axis, and a large movement error of approximately 30 μm in the vicinity of 10.6 s was the influence of the second axis. Furthermore, simulating the movement of each axis in the *Z*-axis direction, revealed that there was almost no error in the movement of the *A*-axis, and the movement of the second axis had a great influence. Thus, the motion error of the second axis caused by reversal motion greatly affects the cutter marks generated in the BCS coordinate system.

3.2. Machining Result in *Y*-Axis Direction

Figure 10 shows the machined surface and the undulation of the processed surface. As shown in the figure, the cutter mark of stripe patterns was observed on the machined surface in the *Y*-axis direction machining. **Fig. 11** shows the machined surface (an area enclosed by squares in **Fig. 10**) magnified by a digital microscope. The cause of the stripe pattern on the machined surface is considered to be the small change in the tool posture, which causes the feed mark to change on machined surfaces A and C.

To clarify the cause of the cutter mark, the change in the velocity of each axis of the machine tool was measured using the internal linear encoder and the controller of the machine tool. As a result, the velocity of the 2nd-axis accelerated and decelerated periodically, as shown in **Fig. 12**. **Fig. 13** shows the relationship between the undulation of the machined surface and the velocity of the second axis. During motion (1) shown in **Fig. 13**, the angle of the tool changed from back to front in the feed direction. During motion (2), the angle of the tool was inclined forward. It is considered that a change in the velocity of the second axis during motion (3) caused the tool to tilt forward again. Thus, the machined surface changed, as shown in C in **Fig. 10**. In motion (4), the tool angle changed from forward to backward as the velocity of the second axis increased rapidly. As a result, the surface undulation also rapidly increased.

The cause of the velocity change in the second axis can be detected but is still not clear in the present situation. It is planned to continue this study by applying the forward kinematics model in this case.

4. Conclusions

A 3D geometric model was derived for a robot-type machine tool with a structure combining serial and parallel link mechanisms. Based on the model, the forward kinematics model was derived to calculate the tool coordinates.

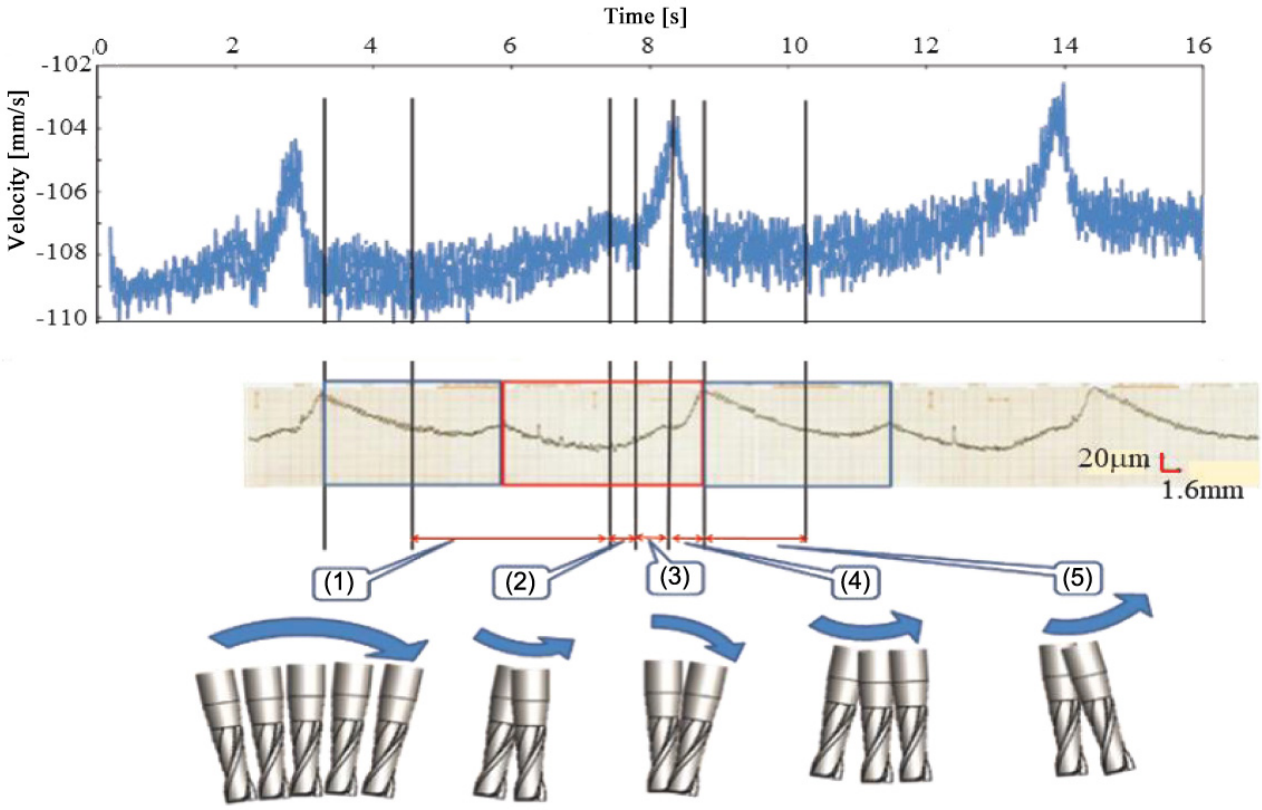

Fig. 13. Image of change of tool posture.

The simulation results of the tool tip coordinate when linear motion was performed and the measurement results from the coordinate measuring machine were compared. It was found that the tool tip position coordinates can be simulated with sufficient accuracy by the proposed model.

As a result of machining tests, different types of cutter mark were found on the machined surface in each X- and Y-axis directions. The calculated results of the motion using the forward kinematics model and measurement results of the velocity of each axis clarified that the cause was the reversal motion of the second axis and A-axis. In particular, the irregular speed change of the second axis generated a unique cutter mark on the machined surface. The proposed model can clarify the influence of the motion of each axis separately. To use this robot-type machine tool for contouring in face milling, it is necessary to suppress such speed change or reversal motion with sufficiency accuracy.

In future work, from the simulation results of the arc motion and the machining result obtained by the actual machining test, it is planned to confirm the roundness and quadrant protrusion and to evaluate the machining performance of this machine and the validity of the model. An inverse kinematics model, the control of a machine that combines both models, and higher precision machining should be investigated in further work.

Acknowledgements

This work was supported by Exechon Enterprises LLC, Giken Co., Ltd., and BBS Kinmei Co., Ltd. The authors would like to thank them for their support.

References:

[1] K. Thoben, S. Wiesner, and T. Wuest, ""Industrie 4.0" and Smart Manufacturing – A Review of Research Issues and Application Examples," Int. J. Automation Technol., Vol.11, No.1, pp. 4-16, 2017.

[2] Y. Domae, "Recent Trends in the Research of Industrial Robots and Future Outlook," J. Robot. Mechatron., Vol.31, No.1, pp. 57-62, 2019.

[3] M. Weck and D. Staimer, "Parallel Kinematic Machine Tools – Current State and Future Potentials," CIRP Annals, Vol.51, No.2, pp. 671-683, 2002.

[4] K. Neumann, "The key to aerospace automation," SAE Aerospace Manufacturing and Automated Fastening Conf. and Exhibition, 2006-01-3144, 2006.

[5] K. Neumann, "Practical and Portable Automated Machining," SAE Aerospace Manufacturing and Automated Fastening, 2014-01-2275, 2014.

[6] S. Matsuoka, K. Shimizu, N. Yamazaki, and Y. Oki, "High-speed End Milling of an Articulated Robot and Its Characteristics," J. of Materials Processing Technology, Vol.95, Issues 1-3, pp. 83-89, 1999.

[7] T. Oiwa, "Precision Mechanism Based on Parallel Kinematics," J. of the Robotics Society of Japan, Vol.4, No.4, pp. 326-336, 2010.

[8] L. B. da Silva, H. Yoshioka, H. Shinno, and J. Zhu, "Tool Orientation Angle Optimization for a Multi-Axis Robotic Milling System," Int. J. Automation Technol., Vol.13, No.5, pp. 574-582, doi: 10.20965/ijat.2019.p0574, 2019.

[9] W. Guo, R. Li, C. Cao, and Y. Gao, "Kinematics Analysis of a Novel 5-DOF Hybrid Manipulator," Int. J. Automation Technol., Vol.9, No.6, pp. 765-774, doi: 10.20965/ijat.2015.p0765, 2015.

[10] G. Ma, Y. Chen, Y. Yao, and J. Gao, "Kinematics and Singularity Analysis of a Four-Degree-of-Freedom Serial-Parallel Hybrid Manipulator," J. Robot. Mechatron., Vol.29, No.3, pp. 520-527, 2017.

[11] T. Harada and K. Dong, "Mechanical Design and Control of 3-DOF Active Scanning Probe Using Parallel Link Mechanism," Int. J. Automation Technol., Vol.5, No.2, pp. 86-90, doi: 10.20965/ijat.2011.p0086, 2011.

[12] Y. Takeda, K. Kamiyama, Y. Maki, M. Higuchi, and K. Sugimoto, "Development of Position-Orientation Decoupled Spatial In-Parallel Actuated Mechanisms with Six Degrees of Freedom," J. Robot. Mechatron., Vol.17, No.1, pp. 59-68, 2005.

[13] K. Xing, J. Mayer, and S. Achiche, "Impact of Model Complexity in the Monitoring of Machine Tools Condition Using Volumetric Errors," Int. J. Automation Technol., Vol.14, No.3, pp. 369-379, 2020.

[14] B. Montavon, P. Dahlem, M. Peterek, and R. Schmitt, "A Digital Perspective on Machine Tool Calibration," Int. J. Automation Technol., Vol.14, No.3, pp. 360-368, 2020.

[15] S. Ibaraki, S. Goto, K. Tsuboi, N. Saito, and N. Kojima, "Kinematic modeling and error sensitivity analysis for on-machine five-axis laser scanning measurement under machine geometric errors and workpiece setup errors," Int. J. of Advanced Manufacturing Technology, Vol.96, pp. 4051-4062, 2018.

[16] S. Ibaraki and I. Yoshida, "A five-axis machining error simulator for rotary-axis geometric errors using commercial machining simulation software," Int. J. Automation Technol., Vol.11, No.2, pp. 179-187, doi: 10.20965/ijat.2017.p0179, 2017.

[17] R. Sato, S. Hasegawa, K. Shirase, M. Hasegawa, A. Saito, and T. Iwasaki, "Motion Accuracy Enhancement of Five-Axis Machine Tools by Modified CL-Data," Int. J. Automation Technol., Vol.12, No.5, pp. 699-706, 2018.

[18] R. Sato, K. Morishita, I. Nishida, K. Shirase, M. Hasegawa, A. Saito, and T. Iwasaki, "Improvement of Simultaneous 5-Axis Controlled Machining Accuracy by CL-Data Modification," Int. J. Automation Technol., Vol.13, No.5, pp. 583-592, 2019.

[19] R. Sato, M. Maegawa, G. Tashiro, and K. Shirase, "Influence of Servo Characteristics on Motion Accuracy of Parallel Kinematic Mechanism," Key Engineering Materials, Vols.523-524, pp. 762-767, 2012.

[20] Y. Oba and Y. Kakinuma, "Simultaneous tool posture and polishing force control of unknown curved surface using serial-parallel mechanism polishing machine," Precision Engineering, Vol.49, pp. 24-32, 2017.

[21] H. Yachi and H. Tachiya, "Calibration Method for a Parallel Mechanism Type Machine Tool by Response Surface Methodology – Consideration via Simulation on a Stewart Platform Mechanism –," Int. J. Automation Technol., Vol.4, No.4, pp. 355-363, 2010.

[22] N. Zimmermann and S. Ibaraki, "Self-calibration of rotary axis and linear axes error motions by an automated on-machine probing test cycle," The Int. J. of Advanced Manufacturing Technology, Vol.107, pp. 2107-2120, 2020.

[23] S. Aoyagi, M. Suzuki, T. Takahashi, J. Fujioka, and Y. Kamiya, "Calibration of Kinematic Parameters of Robot Arm Using Laser Tracking System: Compensation for Non-Geometric Errors by Neural Networks and Selection of Optimal Measuring Points by Genetic Algorithm," Int. J. Automation Technol., Vol.6, No.1, pp. 29-37, doi: 10.20965/ijat.2012, 2012.

[24] S. Ibaraki, T. Yokawa et al., "A Study on the Improvement of Motion Accuracy of Hexapod-type Parallel Mechanism Machine Tool (3rd Report) – A Kinematic Calibration Method Considering Gravity Errors –," J. of JSPE, Vol.72, No.3, pp. 355-359, doi: 10.2493/jspe.72.355, 2004 (in Japanese).

[25] K. Nagao, N. Fujiki, Y. Morimoto, and A. Hayashi, "Calibration Method of Parallel Mechanism Type Machine Tools," Int. J. Automation Technol., Vol.14, No.3, pp. 429-437, doi: 10.20965/ijat.2020.p0429, 2020.

[26] I. Inasaki, "Theory of Generating Motion for Machine Tools: Formulation and Application," JSME Int J., Series C, Vol.60, No.574, pp. 1891-1895, 1994 (in Japanese).

Name:
Akio Hayashi

Affiliation:
Assistant Professor, Kanazawa Institute of Technology

Address:
7-1 Ohgigaoka, Nonoichi, Ishikawa 921-8501, Japan

Brief Biographical History:
2014 Received Ph.D. in Engineering from Graduate School of Engineering, Kobe University
2014- Assistant Professor, Kanagawa University
2017- Assistant Professor, Kanazawa Institute of Technology

Main Works:
• "Simulation of Energy Consumption of Machine Tool Motion for 3-Axis Machining," J. of Energy and Power Engineering, Vol.11, pp. 37-43, 2017.
• "Rotational speed control system of water-driven spindle," J. of the Int. Societies for Precision Engineering and Nanotechnology, Vol.51, pp. 88-96, 2017.

Membership in Academic Societies:
• Japan Society of Mechanical Engineers (JSME)
• Japan Society for Precision Engineering (JSPE)

Name:
Hiroto Tanaka

Affiliation:
Graduate Student, Kanazawa Institute of Technology

Address:
7-1 Ohgigaoka, Nonoichi, Ishikawa 921-8501, Japan

Brief Biographical History:
2020 Received Bachelor of Science in Engineering from Kanazawa Institute of Technology

Membership in Academic Societies:
• Japan Society for Precision Engineering (JSPE)

Name:
Masato Ueki

Affiliation:
Sumitomo Wiring Systems, Ltd.

Address:
5-28 Hamada-cho, Yokkaichi, Mie 510-8528, Japan

Brief Biographical History:
2018 Graduated from Kanazawa Institute of Technology
2020 Graduated from Graduate School of Kanazawa Institute of Technology
2020- Sumitomo Wiring Systems, Ltd.

Main Works:
• Manufacture and sales of wiring harnesses, harness components, and other electric wires

Name:
Hidetaka Yamaoka

Affiliation:
Associate Professor, Mathematics and Science Academic Foundations Programs, Kanazawa Institute of Technology

Address:
7-1 Ohgigaoka, Nonoichi, Ishikawa 921-8501, Japan

Brief Biographical History:
2005 Received Ph.D. from Department of Applied Mathematics and Physics, Graduate School of Informatics, Kyoto University
2006- Research Scientist, VCAD System Research Program, The Institute of Physical and Chemical Research (RIKEN)
2012- Lecturer, Kanazawa Institute of Technology
2017- Associate Professor, Kanazawa Institute of Technology

Main Works:
• "Rotational-Vibrational Energy Spectra of Triatomic Molecules Near Relative Equilibria," J. of Mathematical Physics, Vol.49, 043505, 2008.
• "Continuum Dynamics on A Vector Bundle for A Directed Medium," J. of Physics A: Mathematical and Theoretical, Vol.43, 325209, 2010.
• "Practice of Calculus Lecture Using Peer Instruction by Audience Response System," Proc. of the 2020 11th Int. Conf. on E-Education, E-Business, E-Management, and E-Learning (IC4E 2020), pp. 279-283, 2020.

Membership in Academic Societies:
• Mathematical Society of Japan (MSJ)
• Japanese Society for Engineering Education (JSEE)

Name:
Nobuaki Fujiki

Affiliation:
Associate Professor, Kanazawa Institute of Technology

Address:
7-1 Ohgigaoka, Nonoichi, Ishikawa 921-8501, Japan

Brief Biographical History:
1992- Nachi-Fujikoshi Corp.
1999- Assistant, Kanazawa Institute of Technology
2008- Associate Professor, Kanazawa Institute of Technology

Main Works:
• "Bilateral Servo Mechanisms via Adaptive Control," J. of the Japan Society for Precision Engineering, Vol.68, No.6, pp. 806-810, 2002.

Membership in Academic Societies:
• Japan Society of Mechanical Engineers (JSME)
• Robotics Society of Japan (RSJ)

Name:
Yoshitaka Morimoto

Affiliation:
Professor, Kanazawa Institute of Technology

Address:
7-1 Ohgigaoka, Nonoichi, Ishikawa 921-8501, Japan

Brief Biographical History:
1983- Research Worker, Industrial Research Institute of Ishikawa
1996- Associate Professor, Toyama National College of Technology
1999- Associate Professor, Utsunomiya University
2008- Professor, Kanazawa Institute of Technology
2013- Director, Advanced Materials Science Research and Development Center, Kanazawa Institute of Technology
2016- Dean of Academic Affairs, Kanazawa Institute of Technology

Main Works:
• "Vibration Control of Relative Tool-Spindle Displacement for Computer Numerically Controlled Lathe with Pipe Frame Structure," ASME J. of Manufacturing Science and Engineering, Vol.136, No.4, Paper No: MANU-13-1072; doi: 10.1115/1.4027594, 2012.

Membership in Academic Societies:
• American Society of Mechanical Engineers (ASME)
• Japan Society of Mechanical Engineers (JSME)
• Japan Society for Precision Engineering (JSPE)